Applied Physics Letters

RESEARCH ARTICLE | APRIL 10 2023

Strain effects on the electronic and magnetic properties of Cr_2TaC_2 and $Cr_2TaC_2O_2$ monolayers

Special Collection: MXenes - Physics and Devices

Fuat Bilican; Sevgi Ozdemir Kart; Erol Vatansever; ... et. al

Check for updates

Appl. Phys. Lett. 122, 151901 (2023)
https://doi.org/10.1063/5.0142420

View Online
Export Citation
CrossMark

Downloaded from http://pubs.aip.org/aip/apl/article-pdf/doi/10.1063/5.0142420/16820947/151901_1_5.0142420.pdf

Lake Shore CRYOTRONICS
CryoComplete
A total solution for low-temperature characterization
Learn more ›



AIP Publishing

Applied Physics Letters ARTICLE scitation.org/journal/apl

Strain effects on the electronic and magnetic properties of Cr_2TaC_2 and $Cr_2TaC_2O_2$ monolayers

Cite as: Appl. Phys. Lett. **122**, 151901 (2023); doi: 10.1063/5.0142420
Submitted: 13 January 2023 · Accepted: 23 March 2023 ·
Published Online: 10 April 2023

View Online Export Citation CrossMark

Fuat Bilican,[1] Sevgi Ozdemir Kart,[1] Erol Vatansever,[2] Fatih Ersan,[3,a)] and Zeynep Demir Vatansever[2,a)]

AFFILIATIONS

[1]Department of Physics, Pamukkale University, Denizli 20160, Turkiye
[2]Department of Physics, Dokuz Eylul University, Izmir 35160, Turkiye
[3]Department of Physics, Aydin Adnan Menderes University, Aydin 09010, Turkiye

Note: This paper is part of the APL Special Collection on MXenes - Physics and Devices.
[a)]**Authors to whom correspondence should be addressed:** fatih.ersan@adu.edu.tr and zeynep.demir@deu.edu.tr

ABSTRACT

Double transition metal MXene materials, such as Cr_2TiAlC_2, were successfully synthesized recently in addition to the synthesized mono transition metal MXenes. The physical and chemical properties of the MXenes can be tuned by varying the middle metal layer composition by other metal atoms. Thus, the desired mechanical, electronic, thermal, or magnetic properties can be revealed in that MXene material. The other method to tune material properties is by applying external strain on the structure. In this study, we systematically investigate the physical properties, such as dynamical, thermal, mechanical stability, electronic, and magnetic properties of the Cr_2TaC_2 and the $Cr_2TaC_2O_2$ MXene monolayers for equilibrium and under biaxial strain. We find that both of MXene monolayers are energetically, thermally, and dynamically stable for certain compressive and tensile strain values. The Cr_2TaC_2 and the $Cr_2TaC_2O_2$ MXene monolayers have a ferromagnetic ground state and show a metallic character in an equilibrium state and preserve it up to high tensile strain ($\varepsilon = 0.10$) value. The robust ferromagnetism above room temperature is demonstrated for the Cr_2TaC_2 with a Curie temperature of 714 K for the strain-free case. This value reduces to 234 K for the $Cr_2TaC_2O_2$ monolayer. Moreover, our detailed Monte Carlo simulations reveal that the magnetic transition temperature of the system and also hysteresis properties can be controlled by moving from compressive to tensile strain ratios.

Published under an exclusive license by AIP Publishing. https://doi.org/10.1063/5.0142420

The development of two-dimensional (2D) materials, such as graphene, has opened up a world of possibilities for researchers and engineers.[1–5] By combining different materials, it is possible to create new materials with unique properties that can be used in a variety of applications.[6–13] As research continues, new materials and applications will be discovered, leading to a better understanding of the potential of 2D materials. In recent decades, researchers have been searching for how to use 2D materials in technological applications that could help us have a more sustainable future.[14–18]

Naguib *et al.* synthesized the 2D nanocrystal of Ti_3C_2 material by exfoliating Ti_2AlC_2 at room temperature in hydrofluoric acid[19] and a new member of the 2D family called as MXene is formed. MXenes are 2D layers of early transition metal carbides and/or nitrides. They have been demonstrated to have applications in a wide range of areas, for instance, energy storage, optoelectronics, spintronics, sensing, and biomedicine, thanks to their advanced mechanical, chemical, and electronic properties.[20–23]

MXenes can be found in different forms as single and double-layered Mxenes. Since the first synthesis of Cr_2TiAlC_2 structure by Liu *et al.*,[24] double transition metal Mxenes with the stoichiometry of $M'_2M''C_2$ and $M'_2M''C_3$ (where $M' \neq M'' =$ Nb, Ta, Ti, V, Cr, Mo, etc.) have been widely studied. Particularly, experimental evidence of the magnetic transition in atomically thin $Cr_2TiC_2T_x$ MXene has provided new possibilities to examine the magnetic nature of such materials.[25] Here, the letter T_x indicates the functional groups, such as O, OH, or F atoms. On the theoretical side, Anasori *et al.* proposed dynamically and thermally stable 12 double transition metals MXenes within the framework of density functional theory (DFT).[26] Moreover, robust ferromagnetism has been shown in $Ti_2MnC_2T_x$ monolayers (T = O, OH, and F) and $Hf_2VC_2O_2$ monolayers with high Curie temperatures up to 1133 K.[27] Room temperature ferromagnetism is obtained by Gd-doped in 2D $Ti_3C_2T_x$ MXene.[28] Carbide and nitride MXenes included double transition metals with Cr, Mo, and W considered by Dihingia *et al.*[16] They found various different electronic and magnetic properties with respect to the included atom and surface termination. The studies reported in the literature so far indicate that similar to alloy materials[29,30] double-transition metal MXenes have the opportunity to tune their mechanical, electronic, thermal, and

Downloaded from http://pubs.aip.org/aip/apl/article-pdf/doi/10.1063/5.0142420/16820947/151901_1_5.0142420.pdf

Published under an exclusive license by AIP Publishing

magnetic properties by including other metal atoms in the middle metal layer.

By motivating from the recently synthesized Cr_2TiAlC_2 structure, in this paper, we present a systematic study of the double transition metal MXene: Cr_2TaC_2 and its oxygen functionalized structure $Cr_2TaC_2O_2$ monolayers. Specifically, we investigate the physical properties (dynamical, thermal, and mechanical stability) of the monolayers as well as their electronic and magnetic properties under the biaxial strain. To the best of our knowledge, there is no detailed study about Cr_2TaC_2 and $Cr_2TaC_2O_2$ monolayers in the literature except for a recently published study that focuses on its mechanical properties without considering localized atoms and magnetic properties of the structure.[31] Therefore, we believe that a detailed theoretical investigation of this structure still deserves particular attention.

With the aim of investigating the dynamical, thermal, and mechanical stability of the Cr_2TaC_2 and $Cr_2TaC_2O_2$ monolayers, we use the first-principle calculations based on DFT.[33] In addition, the electronic and magnetic properties of the equilibrium and the strained $Cr_2TaC_2/Cr_2TaC_2O_2$ structures are systematically examined. To study the magnetic features of the $Cr_2TaC_2/Cr_2TaC_2O_2$ structures, we consider the 2D classical anisotropic Heisenberg model. The general Hamiltonian describing the system can be written as

$$H = H_{int} + H_{anis} + H_{Zeeman}. \quad (1)$$

Here, H_{int}, H_{anis}, and H_{Zeeman} terms represent the spin–spin interaction, magnetic anisotropy, and the Zeeman energy, respectively. The model defined in Eq. (1) has been studied by Monte Carlo (MC) simulations based on a single spin-flip Metropolis algorithm.[34–37] Necessary input parameters are obtained by mapping the DFT energies obtained for different magnetic configurations to the Heisenberg spin Hamiltonian. The details for DFT and MC calculations are given in the supplementary material.

We first investigated the bare Cr_2TaC_2 monolayer for the sake of the comparison before applying the biaxial strain to the Cr_2TaC_2 structure. Figure 1(a) shows the top and side views of the Cr_2TaC_2 monolayer with the optimized bond lengths. The calculated optimized lattice constants are $a = b = 3.16$ Å (without Hubbard + U parameter $a = b = 3.10$ Å). The bond lengths between the Ta–C and Cr–C atoms are $d_{(Ta-C)} = 2.26$ and $d_{(Cr-C)} = 2.12$ Å. Bader charge analysis indicates 0.80 and 1.84 e^- transfer from Cr to C and from Ta to C atoms. To obtain the terminated MXene structure, we decorated to the upper and lower surfaces of Cr_2TaC_2 monolayer with O functional group. As illustrated in Fig. S1, three possible adsorption sites are considered and the $Cr_2TaC_2O_2$ monolayers are fully optimized to determine the favorable adsorption site. Our results showed that the highest adsorption energy with the 6.57 eV for per O atom can obtain when O atoms are located on Ta atoms. Figure 1(b) shows the top and side views of the $Cr_2TaC_2O_2$ monolayer with the optimized bond lengths. The calculated optimized lattice constants are $a = b = 3.11$ Å (without Hubbard + U parameter $a = b = 2.96$ Å). With the comparison of the bond lengths between the bare and oxygen-functionalized MXene structures, we see that the Cr–C bond lengths are elongated while the Ta–C bond lengths are shortened after the oxygenation process. Bader charge analysis indicates that the charge transfer from Cr to C and Ta atoms to C atoms increases and each C atoms take 3.17 e^- while the O atoms take 1.10 e^-. We note that all these results are in good agreement with the literature.[31,32]

After the geometric optimization, we evaluate the stability of Cr_2TaC_2 and $Cr_2TaC_2O_2$ monolayers. First, we estimate both the cohesive energy (E_{coh}) and formation energy (E_{FE}) per atom. The E_{coh} is determined from the following expression:

$$E_{coh} = (2E_{Cr} + E_{Ta} + 2E_C - 2E_O - E_{Cr_2TaC_2/Cr_2TaC_2O_2})/n. \quad (2)$$

Here, E_{Cr}, E_{Ta}, E_C, and E_O represent the total energy of an isolated Cr, Ta, C, and O atom, and n is for the number of atoms in the unit-cell,

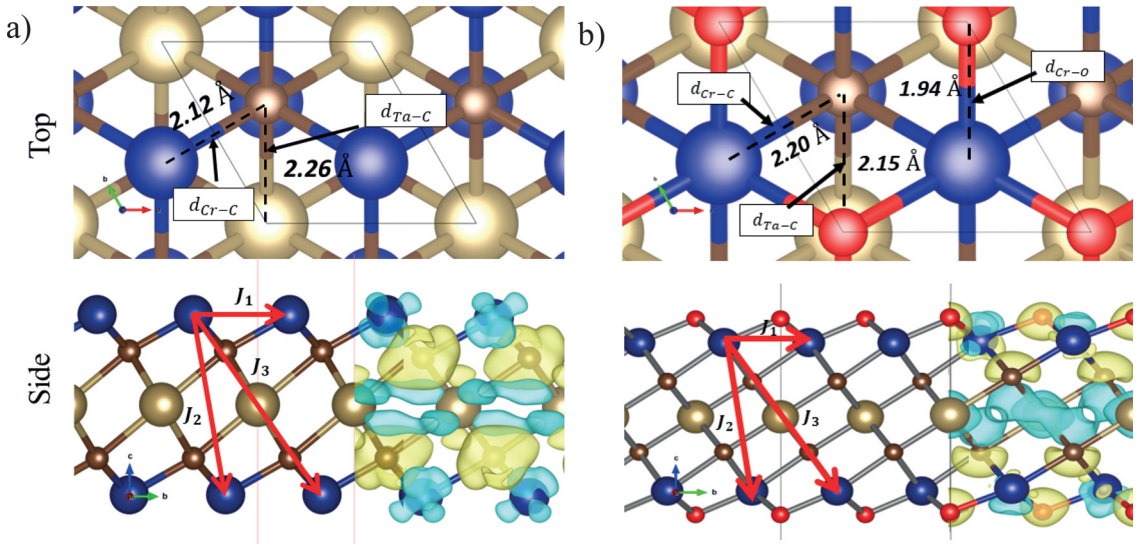

FIG. 1. Top and side views of (a) Cr_2TaC_2 and (b) $Cr_2TaC_2O_2$ structures. The bond lengths of these structures are shown in the figure. Blue, cream, brown, and red spheres indicate Cr, Ta, C, and O atoms, respectively. Charge density difference of Cr_2TaC_2 and $Cr_2TaC_2O_2$ unit-cells, light blue (depletion) and yellow (accumulation) colors indicate charge density. The solid boxes represent unit cells. The density difference isosurface value for Cr_2TaC_2 and $Cr_2TaC_2O_2$ is 0.01 and 0.05 e Å^{-3}, respectively. The first, second, and third spin–spin interactions J_1, J_2, and J_3 are illustrated in the side view.

Downloaded from http://pubs.aip.org/aip/apl/article-pdf/doi/10.1063/5.0142420/16820947/151901_1_5.0142420.pdf

Published under an exclusive license by AIP Publishing

respectively. $E_{Cr_2TaC_2/Cr_2TaC_2O_2}$ denotes the total energy of the $Cr_2TaC_2/Cr_2TaC_2O_2$ monolayer. The obtained E_{coh} values are 6.648 and 6.515 eV/atom for Cr_2TaC_2 and $Cr_2TaC_2O_2$ monolayers, respectively. These values are larger than that reported stable monolayer, such as MnS (4.15 eV/atom) and MnSb (3.48 eV/atom) monolayers.[38] The E_{FE} is then estimated as

$$E_{FE} = E_{Cr_2TaC_2(O_2)(monolayer)} - E_{Cr_2TaC_2(O_2)(bulk)}, \quad (3)$$

where $E_{Cr_2TaC_2(O_2)(monolayer)}$ and $E_{Cr_2TaC_2(O_2)(bulk)}$ stand for the cohesive energies of monolayer and bulk $Cr_2TaC_2/Cr_2TaC_2O_2$ structures, respectively. The estimated E_{FE} is −0.479 eV/atom for Cr_2TaC_2 and is −0.025 eV/atom for $Cr_2TaC_2O_2$ monolayer which indicates that the considered monolayers are thermodynamically stable and can be experimentally synthesized and all E_{coh} and E_{FE} values confirm that the Cr_2TaC_2 and the $Cr_2TaC_2O_2$ sheets are energetically stable.

The dynamic stability of the Cr_2TaC_2 monolayer is determined by analyzing the phonon dispersion curves along the high-symmetry lines in the first Brillouin zone. The required condition to obtain a dynamically stable structure at T = 0 K is the vibration frequencies of the structure ($f(\mathbf{k}) = \frac{\Omega(\mathbf{k})}{2\pi}$) should be positive for the whole Brillouin zone [$f(\mathbf{k}) > 0$]. Our calculations showed that there are no imaginary phonon modes in the first Brillouin zone of the Cr_2TaC_2 monolayer which validates the dynamic stability (see Fig. S2 of the supplementary material).

Thermal stabilities of Cr_2TaC_2 and $Cr_2TaC_2O_2$ structures are tested by *ab initio* finite-temperature molecular-dynamics (MD) calculations at 400 K for 5/6 ps. The snapshots of atomic configurations and the plot of total energy vs time step for Cr_2TaC_2 and for $Cr_2TaC_2O_2$ monolayers which is taken from MD simulations are illustrated in Figs. S3 and S4 of the supplementary material, respectively. As seen, the variation of energy per atom with the changing of time is ignorable and there is not any broken bond or reconstruction in the structure which implies that the Cr_2TaC_2 and the $Cr_2TaC_2O_2$ monolayers are also thermally stable materials for the equilibrium states.

Having established the energetic, dynamic, and thermal stability of the MXene monolayers, the magnetic property is then examined. To determine the ground state of the magnetic orientations, we created $1 \times 2 \times 1$ rectangular cell of the Cr_2TaC_2 and the $Cr_2TaC_2O_2$ monolayers and for four different magnetic orientations (see Figs. S5 and S6 of the supplementary material), and we fully optimized each structure until to get of ∼0 kbar pressure on the considered supercells. The spin–spin interactions between the first (J_1), second (J_2), and third (J_3) neighbor magnetic atoms in the Cr_2TaC_2 and the $Cr_2TaC_2O_2$ structures [see Figs. 1(a) and 1(b)] are calculated by mapping the total energies which are obtained from DFT calculations corresponding to four different magnetic orientations to the classical atomistic Heisenberg spin hamiltonian and can be written as given in the supplementary material. Our numerical calculations reveal that the Cr_2TaC_2 and the $Cr_2TaC_2O_2$ monolayers have a robust ferromagnetic (FM) ground state in the equilibrium (see Tables S1 and S2 of the supplementary material).

After obtaining the magnetic ground state of the structure, we start to apply biaxial compressive and tensile strain by 1% of the lattice constants of the Cr_2TaC_2 and the $Cr_2TaC_2O_2$ monolayers. We applied tensile strain, ε, up to 25% and the obtained stress–strain diagram is shown in Fig. 2. The linear part of the curve shows the elastic region which means the material obeys the general Hooke's law and goes up

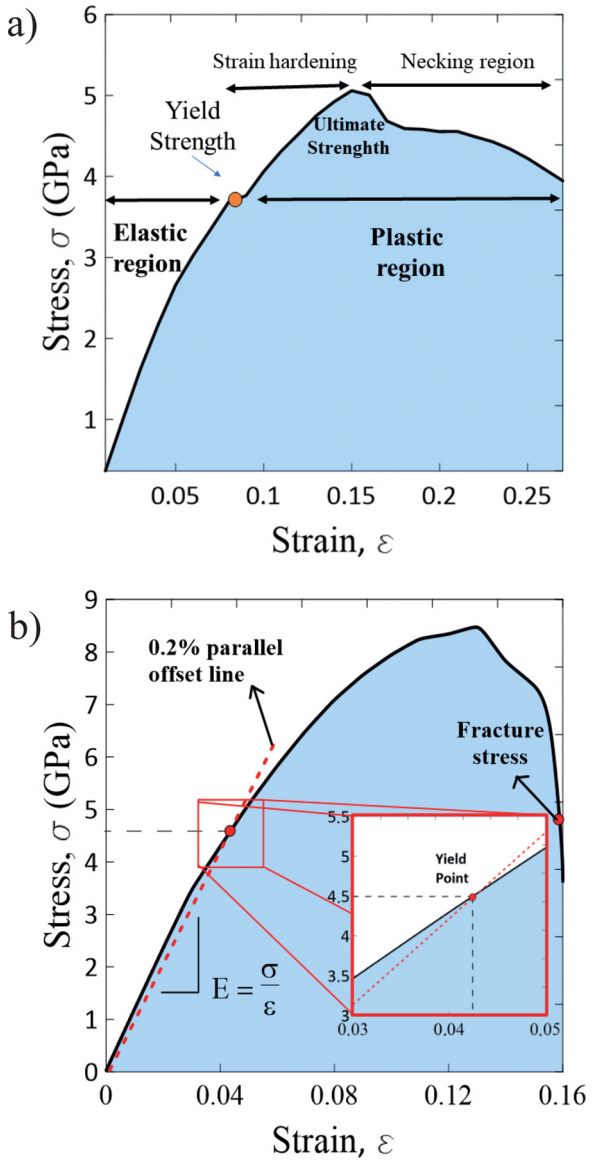

FIG. 2. The biaxial stress–strain relations of the (a) Cr_2TaC_2 and (b) $Cr_2TaC_2O_2$ monolayer.

to 8% tensile strain for Cr_2TaC_2 [Fig. 2(a)]. At 9% tensile strain, there is a hump in the stress–strain curve, which is named the yield point. This yield point indicates the limit of elastic behavior for the Cr_2TaC_2 monolayer and the beginning of plastic behavior which means some fraction of the deformation in the material will be permanent and non-reversible. The other important point in the stress–strain curve is the ultimate tensile strength which means that the maximum stress value of the material can withstand while being stretched or pulled before breaking. This ultimate tensile strength point is close to the yield point for brittle materials, whereas it can be higher in ductile materials. With respect to our results, the Cr_2TaC_2 monolayer may be a ductile material due to the high-level place of the ultimate tensile strength point.

Downloaded from http://pubs.aip.org/aip/apl/article-pdf/doi/10.1063/5.0142420/16820947/151901_1_5.0142420.pdf

Published under an exclusive license by AIP Publishing

However, Jayan *et al.* found that $Mo_2NbC_2O_2$ and $Mo_2TaC_2O_2$ monolayers indicate superior ductility and flexibility with their larger Poisson's ratio when compared to other Cr and Mo-based double transition metal MXenes.[31] Differently from the Cr_2TaC_2, the yield point of the $Cr_2TaC_2O_2$ monolayer is not defined easily from Fig. 2(b). If a yield point is not easily defined from the stress–strain curve similar to our case an offset yield point is arbitrarily defined. To define the arbitrary yield point, first, we found the slope ($E = \frac{\sigma}{\varepsilon}$) of the linear part of the curve, and then we draw a parallel line to this linear part starting from the commonly used strain ratio ($\varepsilon = 0.002$ or 0.2% plastic strain). This method is well defined in the literature by Ross.[39] Our calculations show that the yield point for the $Cr_2TaC_2O_2$ monolayer can be obtained for $\varepsilon = \sim 0.043$, which may imply that the $Cr_2TaC_2O_2$ monolayer can be less robust or stable when we compare it with the Cr_2TaC_2 ($\varepsilon = 0.09$) monolayer. Similar behavior is found by Hatam-Lee *et al.* for Ti_3N_2 and $Ti_3N_2O_2$ monolayers.[40]

Biaxial compressive and tensile strain is applied on the equilibrium FM oriented Cr_2TaC_2 supercell, and the favorable magnetic ground state for each strained Cr_2TaC_2 monolayer is also investigated. Obtained total energies for the corresponding magnetic configurations are given in Table S1 of the supplementary material. Our DFT calculations show that the FM configuration is a ground state from −3% to 9% strain ratio for the Cr_2TaC_2 monolayer and after 9% the antiferromagnetic (AFM) configuration becomes favorable. After determining the magnetic ground state for each structure, we also perform additional calculations to obtain magnetic anisotropy energies of the magnetic ground states (see Tables S3 and S4 of the supplementary material). Furthermore, to verify the stress–strain curve, we performed phonon calculations for strained Cr_2TaC_2 monolayers (see Fig. S3 of the supplementary material). We found that the limit compressive strain value for Cr_2TaC_2 monolayers is −3% and dynamic instability occurs beyond this ratio. However, the Cr_2TaC_2 monolayer is more robust against to tensile strain and dynamically stable until of 9% strain ratio value. Imaginary frequencies in the vicinity of Γ point for the transverse acoustic mode (ZA) arise at 9% strain ratio which corresponds to the yield point shown in Fig. 2. With the increase in the tensile strain ratio, the number of imaginary frequencies increases and all three acoustic modes become imaginary at 12% strain ratio and implying a dynamically unstable Cr_2TaC_2 monolayer. We also performed the MD calculations for the selected strain ratios, such as 8% for Cr_2TaC_2 and 4% and 8% for $Cr_2TaC_2O_2$ monolayers. We obtained that bare Cr_2TaC_2 monolayer is thermally more robust than the oxygen-terminated case due to the occurred reconstruction in $Cr_2TaC_2O_2$ monolayer for the 8% strain ratio value. In addition, there is no reconstruction for 4% strained $Cr_2TaC_2O_2$ structure which confirms the stability that we suggest from the stress–strain curve.

The electronic properties of all considered strained and equilibrium Cr_2TaC_2 and the $Cr_2TaC_2O_2$ monolayers are investigated during this work. Because the considered MXene monolayers involve strongly correlated atoms, the PBE + U calculations are considered in all electronic band structure calculations. The obtained atom-projected band structures are illustrated in Fig. S7 (for Cr_2TaC_2) and in Fig. S8 (for $Cr_2TaC_2O_2$) of the supplementary material. As mentioned above, the equilibrium and strain from −3% to 9% Cr_2TaC_2 monolayer has an FM magnetic ground state, so we separate the electronic band structures as spin-up and spin-down channels. As seen from Fig. S7, the Cr_2TaC_2 monolayer preserves its metallic character against the applied force on the structure. Around the Fermi energy (which is set to zero eV), the orbitals of the Cr atom contribution are dominant for the spin-up channel, while the Ta atoms' orbital contribution is dominant for the spin-down channel for whole considered strained situations. The contribution of C atoms becomes dominant at the lower energy levels (below than −1.5 eV). Similar to the Cr_2TaC_2 monolayer, the $Cr_2TaC_2O_2$ monolayer preserves its FM magnetic ground state and its metallic character against to applied strain from −3% to 8%. However, differently from the bare case, there occurs a gap above the Fermi level around 0.5 to 1 eV, which may shift via electrical field or other external effects and can reveal a semiconductor from the $Cr_2TaC_2O_2$ monolayer.

Next, we examine the magnetic properties of Cr_2TaC_2 and $Cr_2TaC_2O_2$ structures by extensive MC simulations. In Fig. 3, thermal dependencies of magnetization, magnetic susceptibility, and heat capacity are displayed for considered strain values. In MC simulations, the temperature is reduced to 0.1 K, and the magnetic ground state of the structure is determined as FM for strain ratios of −3% to 9% for the Cr_2TaC_2 monolayer. The ground state of the structure becomes AFM with a further increment in the applied strain (10% and 11%). In the case of the $Cr_2TaC_2O_2$ monolayer, the magnetic ground state is determined as FM for all the considered strain values. These findings are also in agreement with the aforementioned DFT predictions. Starting from the value of unity, the magnetization of the structures gradually decreases with increased thermal fluctuations and a second-order phase transition occurs at Curie (Neel) temperature from the ordered FM (AFM) state to the disordered paramagnetic state. The magnetic phase transition can also be observed from the thermal variation of the magnetic susceptibility and specific heat curves. Both of the quantities display a characteristic maximum from which the phase transition temperature of the system is determined.

In Fig. 3, the phase diagrams of the Cr_2TaC_2 and $Cr_2TaC_2O_2$ monolayers in the (T_C/T_N-strain) plane are also displayed. It is obvious that there is a decreasing trend in the transition temperature of the structures when moving from compressive to tensile strain. The decrement in Curie temperature of the structures under strain is clearly due to the reduction in the exchange interaction parameters from the compressive strain to the tensile strain region (see Tables S5 and S6 in the supplementary material) As the exchange interaction between the neighboring magnetic moments weakens, the contribution from the spin–spin interaction term [first term in Eq. (1)] decreases. Therefore, less thermal energy is required to move from the ordered (FM/AFM) state to the disordered (paramagnetic) state resulting in a reduction in the transition temperature. We note that the Curie temperature of the Cr_2TaC_2 monolayer is greater than room temperature up to 8% strain ratio. Also, the exchange interaction parameters (J_1, J_2, J_3) of the monolayer are positive up to 7% strain ratio resulting in FM order. Whereas, the negative values of J_2 and J_3 favor antiparallel alignment of the magnetic moments and hence the existence of AFM order for strain ratios of 10% and 11%. Conversely, Curie temperature of the $Cr_2TaC_2O_2$ monolayer is below the room temperature except for the −3% strain ratio. The transition temperatures and calculated exchange interaction values are given Tables S5 and S6 of the supplementary material.

In Fig. 4, we show the hysteresis loop and coercive field of the Cr_2TaC_2 monolayer for applied strain ratios at room temperature. As one can observe, generally the hysteresis loops have a rectangular

Downloaded from http://pubs.aip.org/aip/apl/article-pdf/doi/10.1063/5.0142420/16820947/151901_1_5.0142420.pdf

Published under an exclusive license by AIP Publishing

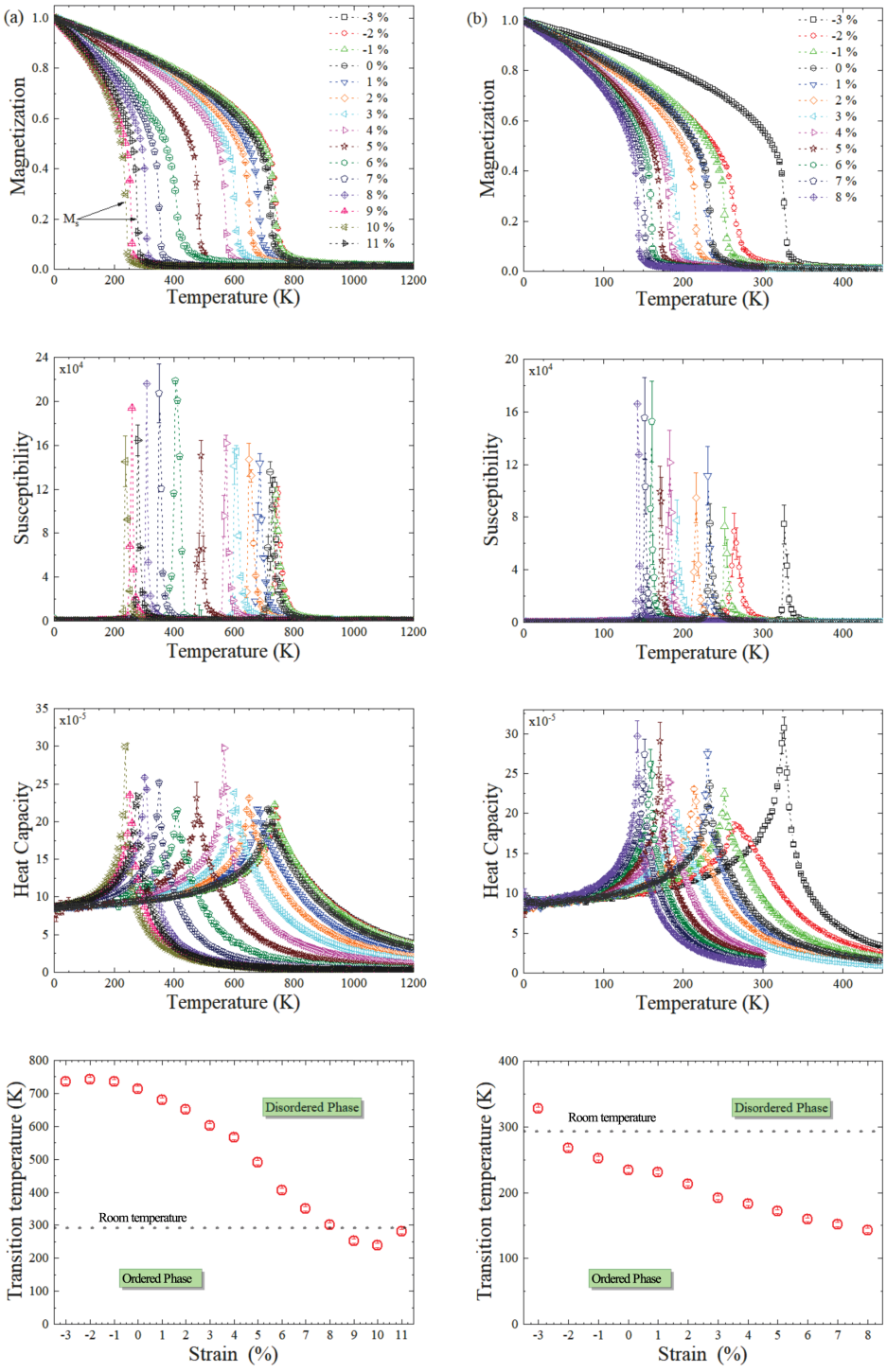

FIG. 3. Magnetic properties of (a) Cr_2TaC_2 and (b) $Cr_2TaC_2O_2$ monolayers under the presence of the applied stress. Thermal dependencies of normalized magnetization (first row), magnetic susceptibility (second row), and heat capacity (third row) are displayed. Here, different symbols correspond to varying applied stress values. The last row presents a magnetic phase diagram in (T_C/T_N-strain) plane. The dashed line refers to the room temperature. The transition points are obtained from the peak positions of the magnetic susceptibility and heat capacity curves. All figures appearing here are collected for $H_{Zeeman} = 0$.

shape. On the other hand, the hysteresis curves are narrower in the case of larger strain values (for instance 6% and 7%). Since the Curie temperature of the structure is below the room temperature for strain ratios of 8% and 9%, S-type hysteresis loops can be explicitly seen. The coercive fields are in the order of meV and, as shown in Fig. 4(b), it represents a non-monotonic behavior for the applied strain values. Room temperature hysteresis curves of $Cr_2TaC_2O_2$ monolayer are given in Fig. 4(c). Since the transition temperature of the monolayer is

Downloaded from http://pubs.aip.org/aip/apl/article-pdf/doi/10.1063/5.0142420/16820947/151901_1_5.0142420.pdf

Published under an exclusive license by AIP Publishing

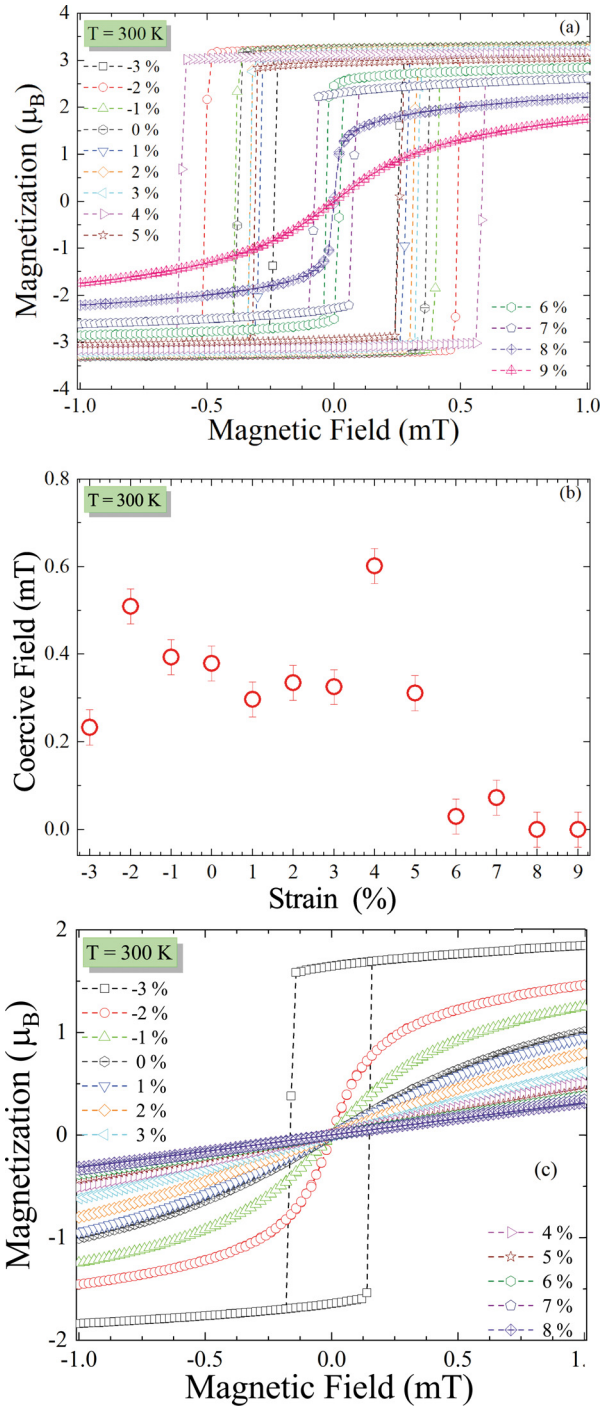

FIG. 4. (a) Hysteresis loop, (b) coercive field of the Cr_2TaC_2 monolayer, and (c) hysteresis loop of the $Cr_2TaC_2O_2$ monolayer as a function of applied strain at 300 K.

lower than the room temperature for all strain values (except the strain ratio of −3%) paramagnetic behavior in the curves can be explicitly observed. Additionally, saturation magnetization values at relatively high fields decrease under strain for both structures.

In summary, our DFT calculations showed that the Cr_2TaC_2 and $Cr_2TaC_2O_2$ monolayers are dynamically, thermally, and mechanically stable double transition metal MXene materials. Cr_2TaC_2 structure has a ferromagnetic ground state with the metallic character electronic property in the equilibrium state. The predicted Curie temperature is 714 K, which implies that the Cr_2TaC_2 monolayer shows robust ferromagnetism above the room temperature when there is no applied stress. In addition, our results revealed that the Cr_2TaC_2 monolayer is dynamically stable up to −3% compressive strain ratio, while this strain value is 9% for tensile strain. A ferromagnetic character with a metallic electronic structure is preserved at −3% to 9% strain values. Moreover, our MC results indicate that it is possible to tune the magnetic properties of the Cr_2TaC_2 monolayer by applied strain. Similar analyses have been also performed for $Cr_2TaC_2O_2$ structure. The numerical results reported in this study show that the $Cr_2TaC_2O_2$ monolayer has a magnetic ground state with the FM character for all studied strain values, but the Curie temperatures found are less than the room temperature except for the −3% strain ratio.

See the supplementary material for the computational details (Figs. S1–S8 and Tables S1–S6).

This work was supported by the Scientific and Technological Research Council of Turkey (TUBITAK) under Research Project No. 121F270. Some parts of the calculations were performed at TUBITAK ULAKBIM High Performance and Grid Computing Center (TR-Grid e-Infrastructure) and the National Center for High-Performance Computing of Turkey (UHEM) under Grant No. 5011222021. F.E. acknowledges some part of DFT calculations to the Aydin Adnan Menderes University Research Fund for providing the high-performance computing facility through Project No. FEF-21021. F.B. acknowledges TUBITAK-BIDEB-2211 Program for the financial support.

AUTHOR DECLARATIONS

Conflict of Interest

The authors have no conflicts to disclose.

Author Contributions

Fuat Bilican: Data curation (equal); Methodology (equal); Writing – original draft (equal). **Sevgi Özdemir Kart:** Methodology (equal); Writing – review & editing (equal). **Erol Vatansever:** Data curation (equal); Formal analysis (equal); Investigation (equal); Methodology (equal); Writing – original draft (equal); Writing – review & editing (equal). **Fatih Ersan:** Data curation (equal); Formal analysis (equal); Investigation (equal); Methodology (equal); Writing – original draft (equal); Writing – review & editing (equal). **Zeynep Demir Vatansever:** Data curation (equal); Formal analysis (equal); Investigation (equal); Methodology (equal); Writing – original draft (equal); Writing – review & editing (equal).

DATA AVAILABILITY

The data that support the findings of this study are available upon reasonable request from the authors.

Downloaded from http://pubs.aip.org/aip/apl/article-pdf/doi/10.1063/5.0142420/16820947/151901_1_5.0142420.pdf

Published under an exclusive license by AIP Publishing

REFERENCES

[1]M. Naguib, O. Mashtalir, J. Carle, V. Presser, J. Lu, L. Hultman, Y. Gogotsi, and M. W. Barsoum, "Two-dimensional transition metal carbides," ACS Nano **6**(2), 1322–1331 (2012).

[2]C. N. R. Rao, K. S. Subrahmanyam, H. S. S. Ramakrishna Matte, B. Abdulhakeem, A. Govindaraj, B. Das, P. Kumar, A. Ghosh, and D. J. Late, "A study of the synthetic methods and properties of graphenes," Sci. Technol. Adv. Mater. **11**(5), 054502 (2010).

[3]T. Sasaki, "Fabrication of nanostructured functional materials using exfoliated nanosheets as a building block," J. Ceram. Soc. Jpn. **115**(1337), 9–16 (2007).

[4]S. Pisana, P. M. Braganca, E. E. Marinero, and B. A. Gurney, "Tunable nanoscale graphene magnetometers," Nano Lett. **10**(1), 341–346 (2010).

[5]K. S. Novoselov, A. K. Geim, S. V. Morozov, D. Jiang, Y. Zhang, S. V. Dubonos, I. V. Grigorieva, and A. A. Firsov, "Electric field effect in atomically thin carbon films," Science **306**(5696), 666–669 (2004).

[6]M. D. Stoller, S. Park, Y. Zhu, J. An, and R. S. Ruoff, "Graphene-based ultracapacitors," Nano Lett. **8**(10), 3498–3502 (2008).

[7]F. Schwierz, "Graphene transistors," Nat. Nanotechnol. **5**(7), 487–496 (2010).

[8]S. Stankovich, D. A. Dikin, G. H. B. Dommett, K. M. Kohlhaas, E. J. Zimney, E. A. Stach, R. D. Piner, S. T. Nguyen, and R. S. Ruoff, "Graphene-based composite materials," Nature **442**(7100), 282–286 (2006).

[9]K. Sato, M. Noguchi, A. Demachi, N. Oki, and M. Endo, "A mechanism of lithium storage in disordered carbons," Science **264**(5158), 556–558 (1994).

[10]M. A. Bizeto, A. L. Shiguihara, and V. R. L. Constantino, "Layered niobate nanosheets: Building blocks for advanced materials assembly," J. Mater. Chem. **19**(17), 2512 (2009).

[11]J. J. Yoo, K. Balakrishnan, J. Huang, V. Meunier, B. G. Sumpter, A. Srivastava, M. Conway, A. L. Mohana Reddy, J. Yu, R. Vajtai, and P. M. Ajayan, "Ultrathin planar graphene supercapacitors," Nano Lett. **11**(4), 1423–1427 (2011).

[12]Y. Yoon, K. Ganapathi, and S. Salahuddin, "How good can monolayer MoS_2 transistors be?," Nano Lett. **11**(9), 3768–3773 (2011).

[13]J. D. Fowler, M. J. Allen, V. C. Tung, Y. Yang, R. B. Kaner, and B. H. Weiller, "Practical chemical sensors from chemically derived graphene," ACS Nano **3**(2), 301–306 (2009).

[14]S. Ali, R. Ali, A. M. Afzal, M. W. Iqbal, M. Hussain, M. Imran, and M. A. Assiri, "Recent advances in 2D-MXene based nanocomposites for optoelectronics," Adv. Mater. Interfaces **9**(31), 2200556 (2022).

[15]B. Anasori, M. R. Lukatskaya, and Y. Gogotsi, "2D metal carbides and nitrides (MXenes) for energy storage," Nat. Rev. Mater. **2**(2), 16098 (2017).

[16]K. D. Dihingia, S. Saikia, N. Yedukondalu, S. Saha, and G. N. Sastry, "2D-double transition metal MXenes for spintronics applications: Surface functionalization induced ferromagnetic half-metallic complexes," J. Mater. Chem. C **10**(47), 17886–17898 (2022).

[17]A. Maleki, M. Ghomi, N. Nikfarjam, M. Akbari, E. Sharifi, M.-A. Shahbazi, M. Kermanian, M. Seyedhamzeh, E. N. Zare, M. Mehrali, O. Moradi, F. Sefat, V. Mattoli, P. Makvandi, and Y. Chen, "Biomedical applications of MXene-integrated composites: Regenerative medicine, infection therapy, cancer treatment, and biosensing," Adv. Funct. Mater. **32**(34), 2203430 (2022).

[18]M. Aghaei, A. A. Sadegh, and B. Panchapakesan, "Experimental and theoretical advances in MXene-based gas sensors," ACS Omega **6**(4), 2450–2461 (2021).

[19]M. Naguib, M. Kurtoglu, V. Presser, J. Lu, J. Niu, M. Heon, L. Hultman, Y. Gogotsi, and M. W. Barsoum, "Two-dimensional nanocrystals produced by exfoliation of Ti_3AlC_2," Adv. Mater. **23**(37), 4248–4253 (2011).

[20]C. Berger, Z. Song, T. Li, X. Li, A. Y. Ogbazghi, R. Feng, Z. Dai, A. N. Marchenkov, E. H. Conrad, P. N. First, and W. A. de Heer, "Ultrathin epitaxial graphite: 2D electron gas properties and a route toward graphene-based nanoelectronics," J. Phys. Chem. B **108**(52), 19912–19916 (2004).

[21]M. J. Allen, V. C. Tung, and R. B. Kaner, "Honeycomb carbon: A review of graphene," Chem. Rev. **110**(1), 132–145 (2010).

[22]A. K. Geim, "Graphene: Status and prospects," Science **324**(5934), 1530–1534 (2009).

[23]A. Hirohata and K. Takanashi, "Future perspectives for spintronic devices," J. Phys. D: Appl. Phys. **47**(19), 193001 (2014).

[24]Z. Liu, E. Wu, J. Wang, Y. Qian, H. Xiang, X. Li, Q. Jin, G. Sun, X. Chen, J. Wang, and M. Li, "Crystal structure and formation mechanism of $(Cr_{2/3}Ti_{1/3})_3AlC_2$ MAX phase," Acta Mater. **73**, 186–193 (2014).

[25]K. Hantanasirisakul, B. Anasori, S. Nemsak, J. L. Hart, J. Wu, Y. Yang, R. V. Chopdekar, P. Shafer, A. F. May, E. J. Moon, J. Zhou, Q. Zhang, M. L. Taheri, S. J. May, and Y. Gogotsi, "Evidence of a magnetic transition in atomically thin $Cr_2TiC_2T_x$ MXene," Nanoscale Horiz. **5**(12), 1557–1565 (2020).

[26]B. Anasori, Y. Xie, M. Beidaghi, J. Lu, B. C. Hosler, L. Hultman, P. R. C. Kent, Y. Gogotsi, and M. W. Barsoum, "Two-dimensional, ordered, double transition metals carbides (MXenes)," ACS Nano **9**(10), 9507–9516 (2015).

[27]L. Dong, H. Kumar, B. Anasori, Y. Gogotsi, and V. B. Shenoy, "Rational design of two-dimensional metallic and semiconducting spintronic materials based on ordered double-transition-metal MXenes," J. Phys. Chem. Lett. **8**(2), 422–428 (2017).

[28]S. Rafiq, S. Awan, R.-K. Zheng, Z. Wen, M. Rani, D. Akinwande, and S. Rizwan, "Novel room-temperature ferromagnetism in Gd-doped 2-dimensional $Ti_3C_2T_x$ MXene semiconductor for spintronics," J. Magn. Magn. Mater. **497**, 165954 (2020).

[29]Y. Z. Abdullahi, A. Bakhtatou, Y. Mogulkoc, and F. Ersan, "Giant band gap bowing in two dimensional Pb_{1-x} Sn_xO alloys and Janus PbSnO monolayers," J. Phys. Chem. Solids **175**, 111203 (2023).

[30]I. Miyazato, S. Sarikurt, K. Takahashi, and F. Ersan, "Controlling electronic structure of single-layered HfX_3 (X = S, Se) trichalcogenides through systematic Zr doping," J. Mater. Sci. **55**(2), 660–669 (2020).

[31]R. Jayan, A. Vashisth, and M. M. Islam, "First-principles investigation of elastic and electronic properties of double transition metal carbide MXenes," J. Am. Ceram. Soc. **105**(6), 4400–4413 (2022).

[32]N. Li, Z. Zeng, Y. Zhang, X. Chen, Z. Kong, Y. Li, P. Zhang, and B.-S. Nguyen, "Double transition metal carbides MXenes (D-MXenes) as promising electrocatalysts for hydrogen reduction reaction: *Ab initio* calculations," ACS Omega **6**(37), 23676–23682 (2021).

[33]P. Hohenberg and W. Kohn, "Inhomogeneous electron gas," Phys. Rev. **136**(3B), B864 (1964).

[34]N. Metropolis, A. W. Rosenbluth, M. N. Rosenbluth, A. H. Teller, and E. Teller, J. Chem. Phys. **21**, 1087 (1953).

[35]*Monte Carlo Methods in Statistical Physics*, edited by K. Binder (Springer, Berlin, 1979), p. 127.

[36]D. P. Landau and K. Binder, *A Guide to Monte Carlo Simulations in Statistical Physics* (Cambridge University Press, Cambridge, 2014), p. 127.

[37]M. E. J. Newman and G. T. Barkema, *Monte Carlo Methods in Statistical Physics* (Oxford University Press, Oxford, 2001), p. 72.

[38]Y. Z. Abdullahi, F. Ersan, Z. D. Vatansever, E. Aktürk, and O. Ü. Aktürk, "Exploring the potential of MnX (S, Sb) monolayers for antiferromagnetic spintronics: A theoretical investigation," J. Appl. Phys. **128**, 113903 (2020).

[39]C. T. F. Ross, *Mechanics of Solids* (Albion/Horwood Publisher, 1999).

[40]S. Milad Hatam-Lee, A. Esfandiar, and A. Rajabpour, "Mechanical behaviors of titanium nitride and carbide MXenes: A molecular dynamics study," Appl. Surf. Sci. **566**, 150633 (2021).

Downloaded from http://pubs.aip.org/aip/apl/article-pdf/doi/10.1063/5.0142420/16820947/151901_1_5.0142420.pdf

Published under an exclusive license by AIP Publishing